

# An Optimal Torque Vectoring Control for Vehicle Applications via Real-Time Constraints

Dhanaraja Kasinathan, Alireza Kasaiezadeh, Andy Wong, Amir Khajepour, Shih-Ken Chen, and Bakhtiar Litkouhi

**Abstract**—A generalized integrated control strategy for vehicle dynamics using an optimal torque vectoring control approach is extended in this paper. The central objective of this approach is to generate optimal additional tire forces and yaw moment over the vehicle through the application of individual wheel torque to keep the vehicle on a target path. This is achieved by minimizing the error between the actual and target forces and moment at the center of gravity (CG). In this paper, this methodology is extended to a constrained optimal control approach that handles additional real-time constraints, which has several vehicle control applications. An online optimization strategy is used to solve the resulting constrained optimization problem that gives the necessary tire force adjustments at the tire level. Some typical applications are 1) differential braking on all wheels, which is applicable to both electric and conventional cars and 2) hybrid torque vectoring on the front wheels and differential braking on the rear wheels. Both simulations and experimental results show the usefulness of this approach of handling constraints with this optimal torque vectoring control.

**Index Terms**—Active-set methods, constrained optimization, differential braking, integrated control, optimal torque vectoring control.

## I. INTRODUCTION

SINCE the 1980s, several advanced chassis control systems have been researched and developed, for instance, active steering, direct yaw moment control (DYC), and active roll control. An active steering system provides additional steer angle to driver commands based on the difference between the expected and actual vehicle response to maintain the vehicle in its desired path. Vehicle lateral stability can be improved using DYC by applying differential braking and traction. However, individual chassis control systems have certain limitations, for instance, in the near saturation region; active steering control cannot generate more tire lateral forces. However, individual chassis control systems have certain limitations, for instance,

in the near tire saturation region, active steering control cannot generate more tire lateral forces due to tire–road friction limits.

Control goals, such as stabilization, ride comfort, and fuel efficiency, have been considered in vehicle dynamics. An integrated control system for active rear-wheel steering and DYC was proposed in [1]. In [2], a nonlinear-optimization-based control for a four-wheel-distributed steering and four-wheel-distributed traction/braking system was proposed. It was shown in [5] that maneuverability in global turning motions can be improved by using an integrated control strategy that coordinates steering and traction. It was shown in [4] that the accuracy of tire force generation is improved using an integrated controller that coordinates DYC and active steering control. A new vehicle dynamics management (VDM) was first proposed in [6], where the target forces and moment of a vehicle are redistributed to each tire to ensure steerability and stability. However, this required tire and slip models due to calculations being performed at the tire force level. In this method, more parameters are required to arrive at a solution. Furthermore, these parameters change as a function of road conditions and tire model. This difficulty can be overcome by directly solving for forces at each wheel hub instead, thus eliminating the necessity for tire models and associated slip ratios. In [24], a unified chassis control strategy by integrating active front steering and electronic stability control designed using Karush–Kuhn–Tucker condition in an optimal manner. Following the desired center of gravity (CG) forces instead of desired yaw rate is studied here as well. Constrained optimization has been used in several papers on vehicle dynamics (see [25]–[34]).

The holistic cornering control (HCC) architecture was originally introduced (see [7] and [8]) as an optimal torque vectoring algorithm that has three objectives: target following, energy minimization, and tire reserve monitoring. It also provides real-time vehicle stability while keeping the vehicle on its intended path at the same time, fault-tolerant capability, and reconfigurability for different vehicles. The evolution of this work was first proposed by a patent filed by General Motors [9]. Following this work, a driver command interpreter (DCI) was developed, and the controller gains were optimized using linear matrix inequalities (LMIs) and genetic algorithm (GA) techniques in [10].

In this paper, the holistic corner control strategy is extended to handle constraints on the tire force adjustments. A preliminary version of this paper can be found in [11]. In this paper, a detailed discussion of HCC and DCI is included. Furthermore, an improved DCI is described. An online active set strategy is used to solve the resulting constrained optimization problem. Some useful applications are 1) differential braking on all of

Manuscript received July 16, 2014; revised January 29, 2015 and May 21, 2015; accepted July 13, 2015. Date of publication August 12, 2015; date of current version June 16, 2016. This work was supported in part by Ontario Research Fund, by Automotive Partnership Canada, and by General Motors. The review of this paper was coordinated by Dr. K. Nam.

D. Kasinathan is with United Technologies Research Center Ireland, Cork, Ireland (e-mail: kasinad@utrc.utc.com).

A. Kasaiezadeh, S.-K. Chen, and B. Litkouhi are with the GM Technical Center, General Motors Company, Warren, MI 48090 USA (e-mail: alireza.kasaiezadeh@gm.com; shih-ken.chen@gm.com; bakhtiar.litkouhi@gm.com).

A. Wong and A. Khajepour are with the Department of Mechanical and Mechatronics Engineering, University of Waterloo, Waterloo, ON N2L3G1, Canada (e-mail: andy.wong@uwaterloo.ca; a.khajepour@uwaterloo.ca).

Color versions of one or more of the figures in this paper are available online at <http://ieeexplore.ieee.org>.

Digital Object Identifier 10.1109/TVT.2015.2467374

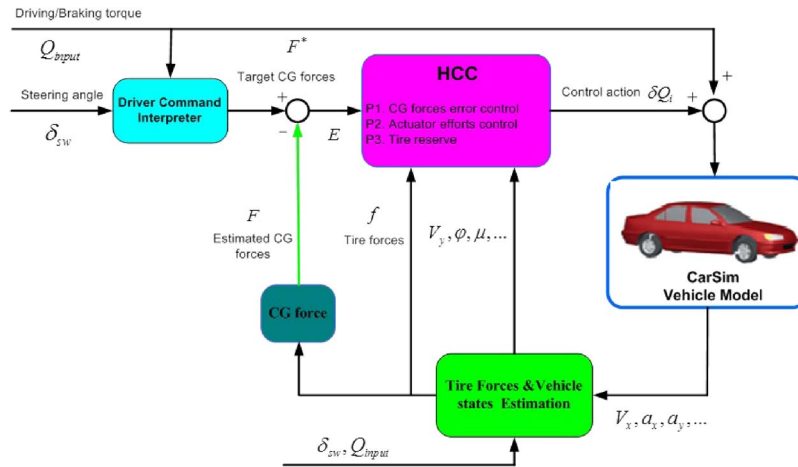


Fig. 1. HCC structure.

the wheels that can be applied to all types of vehicles, either electric or conventional; and 2) hybrid torque vectoring on front wheels and differential braking on the rear wheels. This paper is organized as follows. First, the holistic corner control strategy is described, and then, the control problem is formulated as an unconstrained quadratic optimization problem. Then, we extend this holistic corner control problem to handle constraints on tire force adjustments, which is then demonstrated as a constrained quadratic programming problem. A strategy to solve this constrained optimization problem is then described. Then, the DCI and an improved version of DCI are described. The constrained HCC is shown to work on a full-size vehicle platform, to prove real-world feasibility. The base vehicle for tests in this paper is a 2010 Chevrolet Equinox with stock suspension and tires, modified to be independently driven at each wheel with electric motors. It is meant to be indicative of a production-like SUV. Both simulation and experimental results with both DCI and improved DCI on some typical applications presented here indicate the effectiveness of applying constraints to HCC.

## II. GENERAL STRUCTURE OF THE HOLISTIC CORNER CONTROL

In general, vehicle dynamics can be controlled via wheel torque, steering angles, and suspension forces. A driver controls the vehicle motion using the steering wheel and gas/brake pedals (torque) based on the road conditions. Under poor driving conditions, such as wet and slippery roads or icy roads, the driver might experience difficulty in controlling vehicle motion and in extreme cases, total loss of control. The primary objective of this integrated vehicle control systems is to provide the driver with a normal driving experience under poor road conditions, particularly on icy roads, and to enhance the vehicle stability. Fig. 1 shows the overall structure of the HCC originally proposed in [8] and [9].

The driver's input (steering wheel and gas/brake pedals) are passed to a DCI module. This module applies the driver's input to a vehicle model to generate the desired behavior according to normal driving conditions. It outputs the target vehicle states, which is used to calculate the target (or desired) forces and

moment at the vehicle's CG. The DCI can be replaced by a higher level controller that monitors the vehicle behavior and generate the most feasible target signals that is achievable on any road condition. In such a case, usually, some feedback from vehicle is required. The common feedback for higher level controller includes actual yaw rate (from the inertial measurement unit (IMU) sensor), estimated sideslip angle, and road condition (from estimators). The target values from the DCI are compared against the feedback signals from the actual vehicle response as described by onboard sensors when available or through estimation for signals such as tire force, which cannot be directly measured. Any tuning strategy or vehicle model may be used here, as long as the output of this block provides the target CG forces and moment to the HCC block. Errors between the desired and feedback signals are used to generate corrective signals, which are then input to the HCC block.

Moreover, to ensure that the requested tire forces do not exceed the tire/road capacity, a series of estimations are needed, including longitudinal, lateral, and vertical forces at each tire along with the road condition at each tire contact patch.

The HCC accepts the target-vehicle CG forces and yaw moment as input and generates an output involving torque vectors, suspension forces, or active steering. It generates an additional force and yaw moment over the vehicle by applying individual wheel torque. To achieve the desired CG forces and moment, the tires are controlled by supplementary traction or braking torque, steering angles, and suspension forces (damping in particular). HCC provides the required correction between the actual and the desired path by providing this supplementary traction or braking torque. In the final stage, a summation of the baseline torque from the driver and HCC's supplementary torque is applied to the motor drives.

A quadratic cost function is used to optimize against several parameters, and this optimization problem may be solved either analytically or numerically. The weights within the cost function may be tuned for the vehicle's design objective. Here, emphasis may be placed on any of the following: stability, handling, comfort, energy efficiency, or fault tolerance. Once weighted, this control strategy optimizes against all the requirements in one single step.

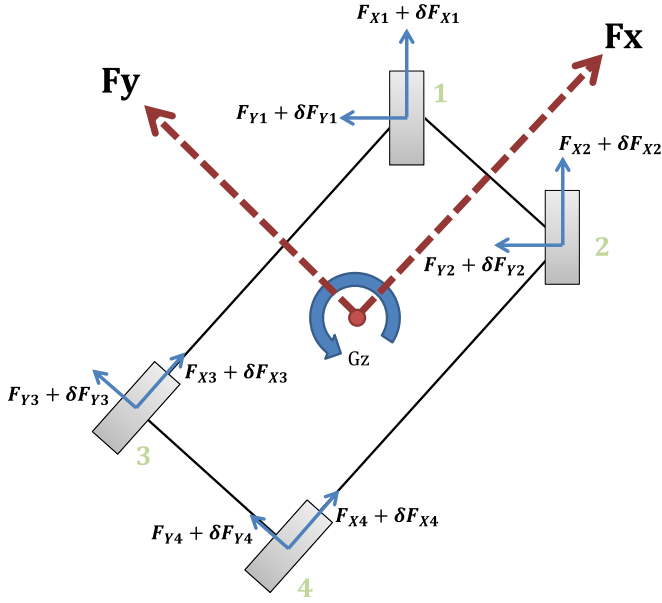


Fig. 2. Force conventions.

### III. HOLISTIC CORNERING CONTROL FORMULATION

The objective of the HCC strategy is to ensure vehicle stability and at the same time follow the desired path. At every time step, the HCC calculates the wheel torque distribution and, whenever necessary, command steer angle adjustments to

- minimize error between target and actual CG forces and moment;
- minimize amplitudes of the control adjustments;
- maximize tire reserves for stabilizing the vehicle.

The desired CG forces obtained from driver's inputs (i.e., steering wheel angle and driving/braking torque values) are denoted by

$$F^* = [F_x^*, F_y^*, G_z^*]^T \quad (1)$$

where  $F_x^*$ ,  $F_y^*$ , and  $G_z^*$  are the desired CG longitudinal force, lateral force, and yaw moment, respectively. The actual forces acting on the CG due to the vehicle motion are denoted by

$$F = [F_x, F_y, G_z]^T \quad (2)$$

where  $F_x$ ,  $F_y$ , and  $G_z$  are the actual longitudinal force, lateral force, and yaw moment acting on the CG of the vehicle. The total tire force vector is defined as

$$\mathbf{f} = [f_1, f_2, \dots, f_8]^T = [F_{x1}, F_{y1}, \dots, F_{x4}, F_{y4}]^T \quad (3)$$

where  $F_{x1}$ ,  $F_{y1}$  are the longitudinal and lateral tire forces on the first tire and so on. The convention for corner numbering is shown in Fig. 2. Each actual CG force component is a function of all tire forces, i.e.,  $F_x(\mathbf{f})$ ,  $F_y(\mathbf{f})$ , and  $G_z(\mathbf{f})$ . The

corresponding adjusted CG forces that reduces the error between the desired  $F^*$  and the actual  $F$  is given as follows:

$$F(\mathbf{f} + \delta\mathbf{f}) \approx F(\mathbf{f}) + \nabla F(\mathbf{f})\delta\mathbf{f}. \quad (4)$$

Here,  $\nabla F(\mathbf{f})$  is a Jacobian matrix that converts the tire-level forces into actual forces at the CG. In the general case,  $\nabla F(\mathbf{f})$  is a matrix of size  $3 \times 8$ , as shown in the following:

$$\nabla F = \begin{bmatrix} \frac{\partial F_x}{\partial F_{x1}} & \frac{\partial F_x}{\partial F_{y1}} & \dots & \frac{\partial F_x}{\partial F_{x4}} & \frac{\partial F_x}{\partial F_{y4}} \\ \frac{\partial F_y}{\partial F_{x1}} & \frac{\partial F_y}{\partial F_{y1}} & \dots & \frac{\partial F_y}{\partial F_{x4}} & \frac{\partial F_y}{\partial F_{y4}} \\ \frac{\partial G_z}{\partial F_{x1}} & \frac{\partial G_z}{\partial F_{y1}} & \dots & \frac{\partial G_z}{\partial F_{x4}} & \frac{\partial G_z}{\partial F_{y4}} \end{bmatrix}. \quad (5)$$

Each element of the Jacobian matrix can be derived using equations of vehicle motion that link the relationship between CG and tire forces. In the general case where all wheels are assumed steerable by angle  $\delta_i$ , the 2-D case becomes

$$F_x = \sum_{i=1}^4 (F_{xi} \cos(\delta_i) - F_{yi} \sin(\delta_i)) \quad (6)$$

$$F_y = \sum_{i=1}^4 (F_{xi} \sin(\delta_i) - F_{yi} \cos(\delta_i)) \quad (7)$$

$$G_z = a \sum_{i=1,2} (F_{xi} \sin(\delta_i) + F_{yi} \cos(\delta_i)) \dots \\ - b \sum_{i=3,4} (F_{xi} \sin(\delta_i) + F_{yi} \cos(\delta_i)) \dots \\ + w \sum_{i=2,4} (F_{xi} \cos(\delta_i) - F_{yi} \sin(\delta_i)) \dots \\ - a \sum_{i=1,3} (F_{xi} \cos(\delta_i) - F_{yi} \sin(\delta_i)). \quad (8)$$

The vector of control actions required to reduce the error between  $F^*$  and  $F$  is defined as follows:

$$\delta\mathbf{f} = [\delta f_{x1}, \delta f_{y1}, \dots, \delta f_{x4}, \delta f_{y4}]^T. \quad (9)$$

In the proposed method, we do not directly control the lateral tire force adjustments. The effect of lateral tire force on the longitudinal dynamics is modeled using the friction circle, which has a direct impact on the applicable brake force, and this is not neglected. It is assumed that there is no means to adjust tire lateral forces directly, and control actions are provided by torque vectoring only; in other words

$$\delta f_{yi} = 0, \quad i = 1, \dots, 4. \quad (10)$$

Therefore, the size of the unknown tire force control vector reduces from 8 to 4. The CG force error vector  $E$  is defined as the difference between actual CG forces and the desired CG forces given by

$$E = [E_x, E_y, E_z]^T = [F_x^* - F_x, F_y^* - F_y, G_z^* - G_z]^T. \quad (11)$$

According to the control goals, the HCC optimization is designed to minimize the following target function:

$$P = \underbrace{\frac{1}{2}(E - \nabla F \delta\mathbf{f})^T W_E (E - \nabla F \delta\mathbf{f})}_{P_1(\delta\mathbf{f})} + \underbrace{\frac{1}{2} \delta\mathbf{f}^T W_{\delta\mathbf{f}} \delta\mathbf{f}}_{P_2(\delta\mathbf{f})} \quad (12)$$

where  $\delta \mathbf{f}$  is the unknown tire force control vector,  $\nabla F$  is the associated Jacobian matrix (5), and  $W_E, W_{\delta \mathbf{f}}$  are weight matrices for CG force error and control effort, respectively. In HCC optimization, this cost function  $P$  (12) is minimized with respect to the tire force adjustment, and the optimal tire force adjustment that is required to reduce the error between actual and desired path is calculated and distributed to the wheel hub as either traction or braking torque vector. The weight matrices  $W_E$  and  $W_{\delta \mathbf{f}}$  are selected such that the objective function  $P$  remains positive definite; the selection will be discussed later. It is assumed here that the tire forces are inside the friction circle. The solution for the minimization problem is derived as follows:

$$\delta \mathbf{f} = [W_{\delta \mathbf{f}} + (\nabla F^T W_E) \nabla F]^{-1} [\nabla F^T (W_E E)]^T \quad (13)$$

provided the following condition is met:

$$\det [W_{\delta \mathbf{f}} + (\nabla F^T W_E) \nabla F] \neq 0. \quad (14)$$

This solution is most commonly referred to as a closed-form solution. After calculating the unknown tire force control vector  $\delta \mathbf{f}$ , differential torque  $\delta Q$  that corresponds to this tire force control vector is calculated using the following:

$$\delta Q_i = R_{\text{eff}} \delta f_i, \quad i = 1, \dots, 4 \quad (15)$$

and applied on all the four wheels, where  $R_{\text{eff}}$  denotes the effective wheel radius.

The primary HCC cost function  $P$  (12) contains matrices that are multiplied against the weights  $W_E$  and  $W_{\delta \mathbf{f}}$ . The first term  $P_1(\delta f)$ , which is controlled by  $W_E$ , applies to the CG force tracking error, and is applied against the error signal. As a result,  $W_E$  is a diagonal matrix where each active element corresponds to one of the axis present in the error vector  $E$ . The 2-D case is defined as follows:

$$W_E = \begin{bmatrix} W_{F_X} & 0 & 0 \\ 0 & W_{F_Y} & 0 \\ 0 & 0 & W_{G_Z} \end{bmatrix}. \quad (16)$$

The second term in the HCC objective function deals with the actuator effort and is governed by  $W_{\delta \mathbf{f}}$ . This term attempts to save energy by preventing excessive use of actuators. The format of this weight is a diagonal matrix, i.e.,

$$W_{\delta \mathbf{f}} = \text{diag}[W_{x_1}, \dots, W_{x_4}] \quad (17)$$

where the individual components correspond to weights on traction motor effort for individual wheels.

We will now rewrite the HCC objective function in the standard quadratic programming format and in Section IV, we will show how to solve this quadratic programming problem [12]. The HCC objective can be rewritten as follows:

$$P = \frac{1}{2} \delta \mathbf{f}^T (W_{\delta \mathbf{f}} + (\nabla F^T W_E) \nabla F) \delta \mathbf{f} - (\nabla F^T (W_E E)) \delta \mathbf{f} + \frac{1}{2} E^T W_E E. \quad (18)$$

The last term in (18) is a constant with respect to the optimizing variable (the adjustment tire force  $\delta f$ ). Note that the minimization problem can also be rewritten in the standard quadratic programming format [12] as follows:

$$\min_{\delta \mathbf{f}} \frac{1}{2} (\delta \mathbf{f})^T H \delta \mathbf{f} + g^T \delta \mathbf{f} \quad (19)$$

where  $H$  is the Hessian matrix, and  $g$  is a vector described in the following:

$$H = W_{\delta \mathbf{f}} + (\nabla F^T W_E) \nabla F, \quad g = -(\nabla F^T (W_E E)). \quad (20)$$

Note that the Hessian matrix  $H$  is positive definite, i.e.,  $H > 0$ . Therefore, this is a convex minimization problem [12]. This guarantees the existence of a unique solution. This solution can either be calculated exactly using the closed-form solution or using numerical techniques that involve an iteration procedure [13].

#### IV. HOLISTIC CORNERING CONTROL WITH CONSTRAINED OPTIMIZATION

The controller design objective in HCC leads to a quadratic programming problem that has a closed-form solution. In this paper, we extend the methodology of HCC to handle real-time constraints on the tire force adjustment. Mathematically, a linear constraint is a convex function. Since both the quadratic programming problem and the linear constraints are convex in nature, the quadratic programming problem subject to linear constraints is also a convex problem [12]. Theoretically, such a linearly constrained quadratic programming problem (21) has a solution, and furthermore, this solution is unique. For example

$$\begin{aligned} \min_{\delta \mathbf{f}} \quad & \frac{1}{2} (\delta \mathbf{f})^T H \delta \mathbf{f} + g^T \delta \mathbf{f} \\ \text{subject to} \quad & G \delta \mathbf{f} \leq b \end{aligned} \quad (21)$$

is a linearly constrained quadratic problem where  $G$  is the constraint matrix and  $b$  is a vector.

In some typical vehicle control applications, the tire force adjustment vector should be restricted (or constrained). For instance, to implement differential braking on all the four wheels, the adjusted tire force control vector should be constrained to be nonpositive. An advantage of adding this constraint enables HCC implementation in conventional cars with mechanical braking since conventional cars do not have electric motors for actuation. Another important vehicle control application is hybrid torque vectoring on the front wheels and differential braking on the rear wheels. In this application, both traction and braking tire force adjustments must be applied on the front wheels, whereas only braking forces must be applied on the rear wheels. Thus, a big advantage of adding constraints to HCC optimization broadens the application of HCC to various special control problems.

##### A. Solution of a Constrained Quadratic Programming Problem

A closed-form solution for an equality-constrained quadratic programming problem has appeared in the optimization literature (see [14] and [15]). Finding a closed-form solution

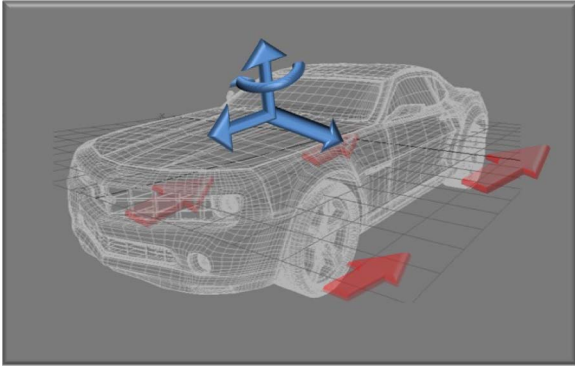


Fig. 3. Differential braking on all wheels (applicable to both conventional and electric cars).

for an inequality-constrained quadratic programming problem or general constrained quadratic programming problem is an open problem in the literature. Analytical methods may exist under specific conditions. Numerical methods are normally the only possible means to solve for the solutions of inequality-constrained optimization problems. For solving constrained optimization problems, wide varieties of numerical methods are used [13], e.g., interior point methods [17], active-set methods [18], augmented Lagrangian methods [19], trust-region reflective methods [20], and other gradient methods [13].

The novelty presented in the following is the application of vehicle control problems to conventional cars with no electric motors for actuation. In this paper, the active-set algorithm given in [13] is used to solve the resulting constrained optimization problem. An implementation of this algorithm can be found in [16].

### B. Applications of Constrained HCC

An application of using HCC with constraints is differential braking on all the four wheels. Differential braking is achieved if the adjusted tire force control vector (on all four tires) is restricted to be nonpositive (see Fig. 3). Mathematically, this can be described as the HCC optimization problem (19) subject to the following constraint:

$$\delta f_{xi} \leq 0, \quad i = 1, \dots, 4. \quad (22)$$

HCC with a differential braking constraint on all wheels can also be written in the form of (21) using  $G = I \in \mathbb{R}^{4 \times 4}$ , with the identity matrix  $b = 0 \in \mathbb{R}^4$ . Therefore, we restrict the HCC controller to apply only the braking torque to all the four wheels, i.e., no traction torque adjustment is applied. When the tire forces are already in the traction mode, HCC is forced to apply no additional traction torque. As a result, the braking torque applied on the tires must compensate to keep the vehicle in the desired path. Note that differential braking with HCC is applicable to all types of vehicles, i.e., conventional, hybrid, and electric.

Another important vehicle control application is hybrid torque vectoring on the front and differential braking on the rear wheels (see Fig. 4). In this application, both traction and braking tire force adjustments must be applied on the front wheels, whereas only braking forces must be applied on the

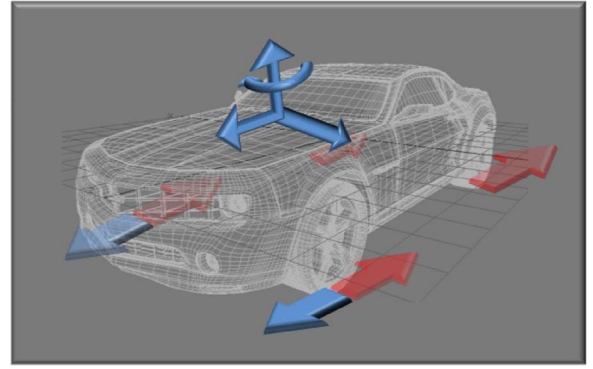


Fig. 4. Hybrid torque vectoring on front wheels and differential braking on rear wheels (applicable for front-wheel drive vehicle).

rear wheels. Mathematically, this constraint can be written as follows:

$$\delta f_{xi} \leq 0, \quad i = 3, 4 \quad (23)$$

which then becomes a constraint on the quadratic objective function (19). Again, this vehicle control problem can be rewritten in the form of (21) by using  $G = \text{diag}(0, 0, 1, 1)$ ,  $b = 0 \in \mathbb{R}^4$ . Thus, it is evident that the advantage of adding constraints broadens the application of HCC to various vehicle control problems.

### V. DRIVER COMMAND INTERPRETER

The DCI module converts the driver's inputs to a target (or desired) state for the HCC to follow. The inputs to the DCI are steering wheel angle, driver torque/brake requests, and current vehicle states. The DCI translates these inputs into desired forces, yaw rate, and moment about the CG. The standard two-degrees-of-freedom bicycle model was chosen for the current implementation of HCC with a linear tire model to generate an ideal yaw rate. However, the actual tire response is nonlinear in high-slip conditions, which leads to an error between this simple model and the feedback signal from the estimation. Such discrepancies are easily handled by HCC since HCC adjusts for the additional traction/braking torque automatically and eliminates any error to realize the ideal vehicle behavior. A single understeer coefficient ( $K_{us}$ ) term is used to tune the vehicle response, encapsulating the impact of virtual cornering stiffness on steering response. This term is defined as [21]

$$K_{us} = \frac{mb}{LC_{\alpha f}} - \frac{ma}{LC_{\alpha r}}. \quad (24)$$

Here,  $a$  represents the distance from CG to the front axle,  $b$  is the distance from CG to the rear axle,  $m$  is the mass of the vehicle, and  $L$  is the total wheel base. Independent values for the front and rear cornering stiffness are defined as  $C_{\alpha f}$  and  $C_{\alpha r}$ , respectively.

The desired yaw rate ( $r_d$ ) of the vehicle is expressed as a function of  $K_{us}$  and the front steered angle  $\delta$  as follows [21]:

$$r_d = \frac{V_x \delta}{L + K_{us} V_x^2}. \quad (25)$$

Thus, the response of the driver can be tuned using the understeer coefficient  $K_{us}$ . Vehicle stability and its response can be adjusted with only one coefficient. In general, a negative  $K_{us}$  results in an oversteering vehicle, whereas a positive value results in understeering.

Note that the yaw rate is an output from the model, whereas the HCC requires yaw moment as the input. The conversion between an ideal yaw rate and actuator moment requires an intermediary controller. There are two major motivations for doing this. First, stock commercial IMUs only provide yaw rate signals to be used as feedback signals. Earlier versions of the DCI attempted to use the time derivative of these signals for moment feedback, but sensor noise caused large errors in the resulting rates. Smoothing filters were attempted, but the time delays encountered in such filters led to laggy response and controller oscillation. Second, a pure moment-based controller is subject to steady-state errors. These reasons combined led to the selection of a rate-based feedback system, followed by a simple proportional controller to command the HCC.

## VI. IMPROVED DRIVER COMMAND INTERPRETER

An improved DCI is described in the following. As the maximum lateral acceleration of any road vehicle depends on the friction coefficient of the road surface, the desired yaw rate should be adjusted as follows [22]:

$$r_d = \min \left( \frac{V_x \delta}{L + K_{us} V_x^2}, \frac{\mu g}{V_x} \right). \quad (26)$$

This helps to prevent excessive body sideslip angle on slippery road conditions. A practical challenge in using (26) is the estimation of road friction  $\mu$  that is not an easy problem to solve. To mitigate this issue, one can replace  $\mu g$  in (26) by lateral acceleration, then (26) will be modified to the following:

$$r_d = \min \left( \frac{V_x \delta}{L + K_{us} V_x^2}, \frac{a_y}{V_x} \right). \quad (27)$$

Although very helpful, (27) does not guarantee that body sideslip angle is under controlled. A standard control strategy for integrated yaw and sideslip angle control is employed in this paper to control yaw rate and sideslip angle simultaneously [23]. Here, we use the error between the desired and actual yaw moment  $E_z = G_z^* - G_z$  as

$$E_z = K_r(r_d - r) + K_\beta(\beta_d - \beta) \quad (28)$$

where  $r_d$  and  $\beta_d$  are the desired yaw rate and sideslip angle, respectively, and  $K_r$  and  $K_\beta$  are tunable controller gains. The desired sideslip  $\beta_d$  can be determined based on a simple bicycle model or simply can be assumed zero, i.e.,  $\beta_d = 0$ . For the simulation and experimental results in the following, we used  $K_r = 15000$  and  $K_\beta = 1000$ .

## VII. SIMULATIONS

The vehicle parameters used in our simulations are shown in Table I. We used the online active-set strategy described earlier to solve the constrained quadratic programming numerically. The weight matrices are chosen in such a way that the tire

TABLE I  
VEHICLE PARAMETERS

Vehicle Width ( $w$ )	1.842 m
Vehicle Height ( $h$ )	1.684 m
Vehicle Wheelbase ( $L$ )	2.858 m
Front CG distance ( $a$ )	1.42 m
Rear CG distance ( $b$ )	1.438 m
Vehicle Mass ( $M$ )	2300 Kg
Effective Wheel Radius ( $R_{eff}$ )	0.365 m

TABLE II  
COMPARING THE SPEED OF CALCULATING A SOLUTION TO THE OPTIMIZATION PROBLEM USING BOTH CLOSED-FORM AND NUMERICAL METHODS

Problem Type	Method	CPU Time	#min iters	#max iters	#mean iters
HCC Optimization	Closed Form	30 $\mu$ s	N/A	N/A	N/A
Constrained HCC <sup>1</sup>	Numerical Form	100 $\mu$ s	4	11	5.94
Constrained HCC <sup>2</sup>	Numerical Form	95 $\mu$ s	0	3	0.53
Constrained HCC <sup>3</sup>	Numerical Form	84 $\mu$ s	0	6	0.02

<sup>1</sup>No initial ansatz is provided

<sup>2</sup>The closed form solution is used as initial ansatz

<sup>3</sup>The solution at the previous time step is used as initial ansatz

adjustment forces are equally distributed on all the wheels, and the error between desired and actual yaw moment at the CG is reduced (see  $W_{F_x} = 0$ ,  $W_{F_y} = 0$ ,  $W_{G_z} = 1$ ,  $W_{x1} = 1$ ,  $W_{x2} = 1$ ,  $W_{x3} = 1$ , and  $W_{x4} = 1$ ). A sampling time of 5 ms was used. Table II compares the speed of closed-form and numerical methods. For the numerical method, the minimum, maximum, and mean numbers of iterations required to calculate the solution starting with no ansatz, closed-form solution, and previous time step solution are shown. The CPU times given in the table are the mean values calculated over 15 000 samples. The mean number of iterations required for solving the constrained HCC when it is initialized with the previous sample solution is significantly less than that initialized with the closed-form solution. In the case of constrained HCC, the solution can be calculated much faster if the previous time-step solution is used as an initial ansatz than using the closed-form solution, which is in turn faster than not providing any initial ansatz at all. Clearly, the time required for computing the numerical solution for the constrained HCC was much less than the sampling time of 5 ms. Thus, the controller calculated the unique solution for the constrained optimization problem successfully at every time step. Fig. 5 shows the driver's steering wheel input for a double-lane change maneuver with an initial speed of 80 km/h. The tire-road friction coefficient is assumed 0.72 if not otherwise mentioned.

### A. Differential Braking

With the differential braking constraint on HCC, when the tire forces are already in the traction mode, HCC is forced to apply no additional traction torque. As a result, the braking torque applied on the tires must compensate to keep the

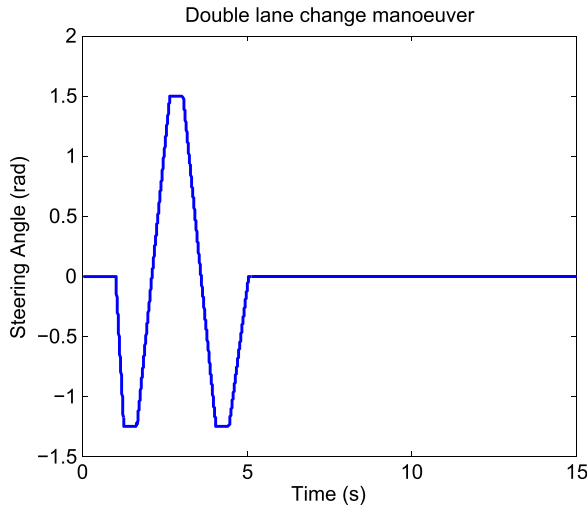


Fig. 5. Driver's wheel steering input.

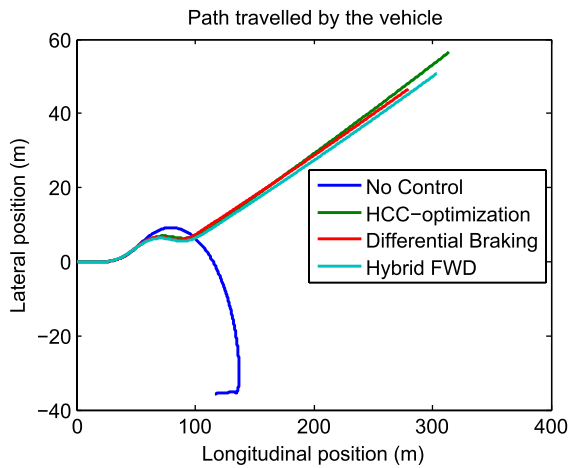


Fig. 6. Path traveled by uncontrolled vehicle, controlled vehicle, and controlled vehicle with differential braking on all wheels and hybrid torque vectoring in the front (FWD) with differential braking on the rear over a surface with  $\mu = 0.72$ .

vehicle in the desired path. It is clear from Fig. 7 that the numerical solution of the differential-braking-constrained HCC generates nonpositive torque on all the wheels at all times. At the 4th second, the differential torque generated by the HCC optimization on the front left, front right, rear left, and rear right wheels are  $-170.2$ ,  $213.9$ ,  $-192.5$ , and  $192.5$   $\text{N} \cdot \text{m}$ , respectively. These values indicate that the vehicle is negotiating a left turn. With the differential braking constraint on HCC, no traction torque is applied on front right and rear right wheels but braking torque values of  $-140.8$   $\text{N} \cdot \text{m}$  and  $-159.1$   $\text{N} \cdot \text{m}$  are applied on front and rear left wheels at the 4th second. These values show that the vehicle is maneuvering a left turn. Fig. 6 shows that the path generated with the constrained HCC is very close to the path generated with the HCC optimization. Note that differential braking with HCC is applicable to all types of vehicles, i.e., conventional, hybrid, and electric.

### B. Hybrid Torque Vectoring and Differential Braking

Another application of using HCC with constraints is for a front-wheel drive vehicle with differential braking on the rear

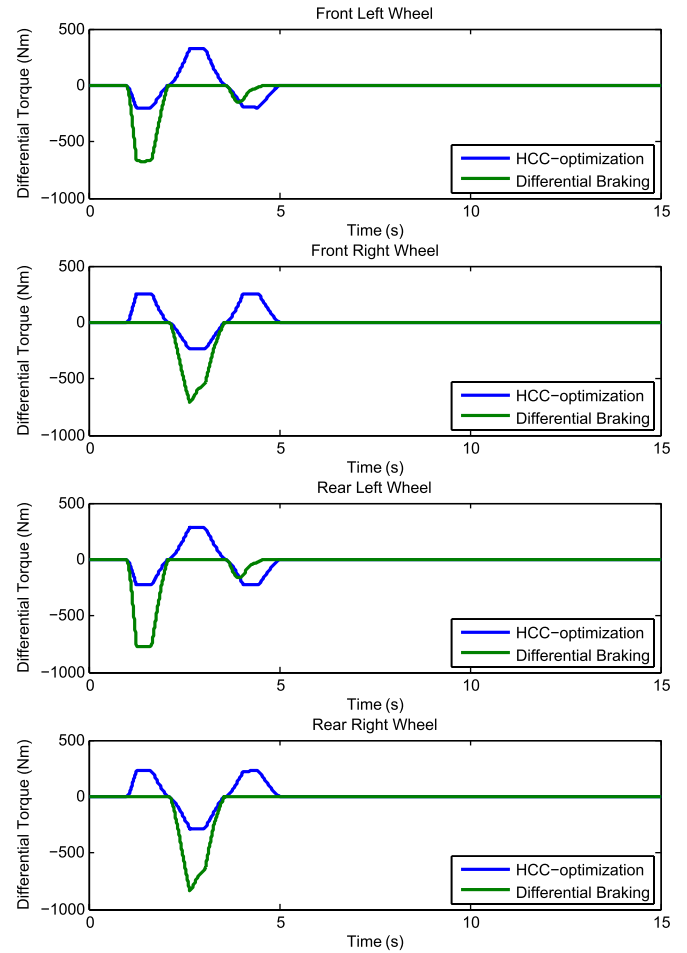


Fig. 7. Simulation: Differential torque generated with HCC optimization and constrained HCC with differential braking on all the wheels.

tires only. This is achieved by restricting the adjusted tire force on the rear wheels to be nonpositive while applying no restriction on the adjusted tire force for the front wheels. It is clear from Fig. 8 that the numerical solution of the hybrid-torque-vectoring-constrained HCC generates nonpositive torque on the rear wheels at all times. The traction torque,  $443.1$   $\text{N} \cdot \text{m}$ , on the front right wheel, the braking torque, i.e.,  $-352.6$  and  $-398.7$   $\text{N} \cdot \text{m}$ , on the front and rear left wheels at the fourth second indicate that the vehicle is maneuvering a left turn. Fig. 6 shows the path generated with the hybrid torque vectoring (FWD) constraint on HCC is very close to the path generated with the HCC optimization. Thus, we restrict the HCC controller to apply just the braking torque on the rear wheels while applying no such restriction on the front wheels (in other words, both traction and braking torque are allowed on the front wheels).

Note that the clipped results in HCC optimization shown in Figs. 7 and 8 is due to the intentional clipping in steering input for double-lane change in Fig. 5. As a result, the desired and actual yaw rate will be clipped at certain points. This means that the error signal may look like the yaw rate, and as the HCC output is proportional to the error, it is not surprising that the HCC outputs are clipped. A careful analysis of the outputs of differential braking and hybrid torque vectoring will show that the clipping also occurs here at some specific points. Because

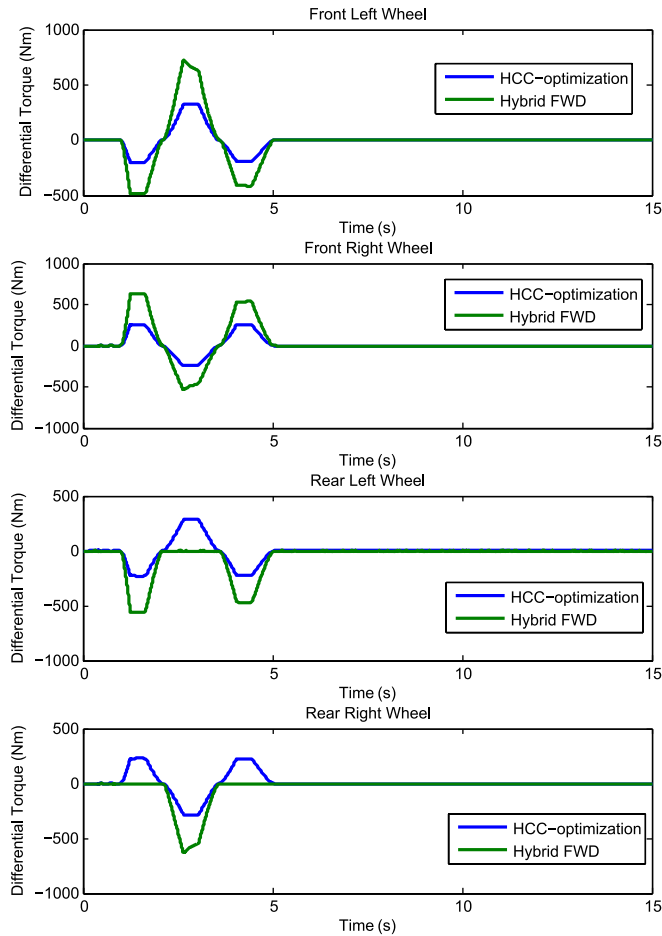


Fig. 8. Simulation: Differential torque generated with HCC optimization and constrained HCC with hybrid torque vectoring on the front wheels (FWD) and differential braking on the rear wheels.

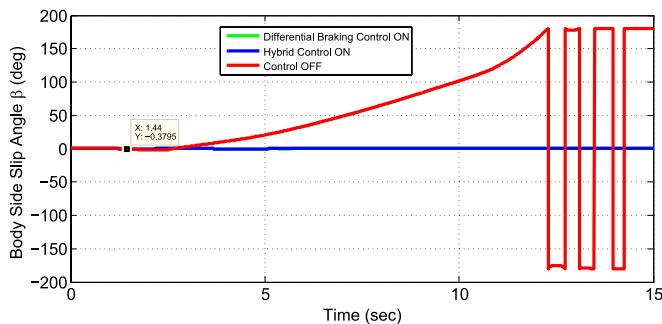


Fig. 9. Simulation: Variation of body sideslip angle over time in a double-lane change maneuver with no control and differential braking and hybrid torque vectoring control on a surface with  $\mu = 0.3$ .

it cannot apply positive torque, to handle the clipped yaw rate error, it may have irregular shape.

With the improved DCI, Fig. 9 shows the change in body sideslip angle with respect to time for a double-lane change maneuver with different controls on a road surface with a low coefficient of friction (see  $\mu = 0.3$ ) at a constant speed of 55 km/h. It is clear that, when the controller is turned off, the sideslip angle becomes unstable. With the differential braking control and hybrid torque vectoring control, the sideslip angle remains very small. Hence, it is important to have the sideslip

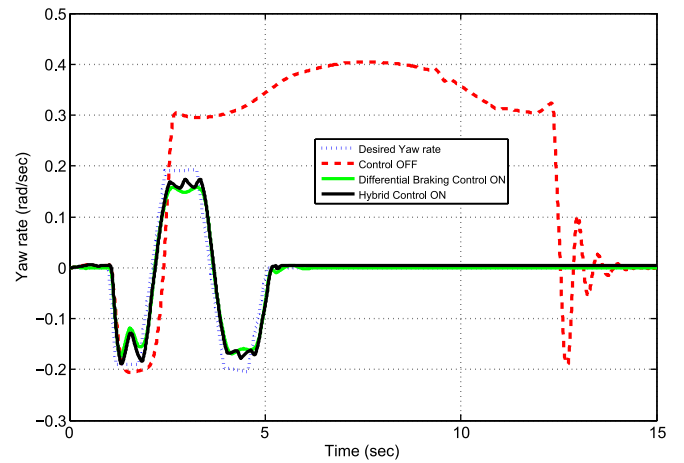


Fig. 10. Simulation: Variation of yaw rate over time in a double-lane change maneuver with no control, and differential braking and hybrid torque vectoring against desired yaw rate on a surface with  $\mu = 0.3$ .

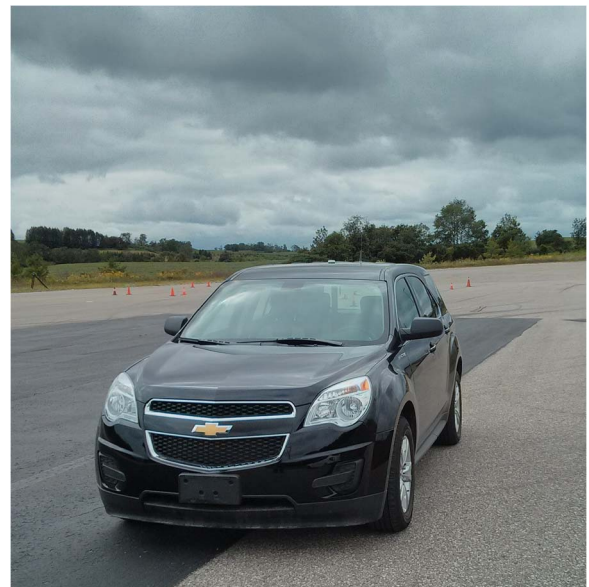


Fig. 11. Test Vehicle: 2010 Chevrolet Equinox.

under control and, more importantly, close to zero as much as possible. For the same road conditions and driving speed, Fig. 10 compares the variation of yaw rate with no control, and control with differential braking and hybrid torque vectoring against the desired yaw rate. Clearly, the yaw rate with the controllers with differential braking constraint and hybrid torque vectoring constraint follows the desired yaw rate but not when the controller is turned off.

### VIII. EXPERIMENTAL RESULTS

The HCC formulation was implemented on both the FWD and 4WD variations of the in-house Equinox test bed (see Fig. 11). In testing, stock all-season Michelin Latitude tires were used, and production sensors provided steering wheel angle, IMU, and wheel speeds. The test vehicle is equipped with a number of sensors including GPS and high-quality IMU for validation. Control code was created in MATLAB Simulink,

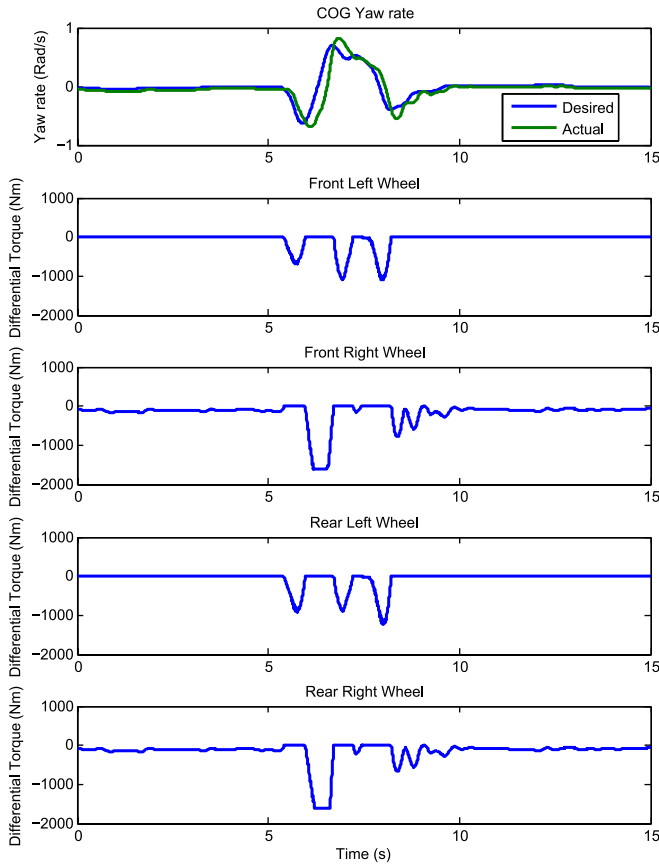


Fig. 12. Experimental result: Differential torque values generated by differential-braking-constrained HCC optimization on all the wheels.

and cross-compiled to run in an embedded dSpace Micro-Autobox controller that is set to a loop cycle rate of 200 Hz. Simulation data are performed by bridging the control code to a CarSim vehicle model that was built using table data from a rig-tested stock Equinox SUV.

An online active-set strategy [16] was used to solve the constrained quadratic optimization problem for a double-lane change maneuver at a speed of 65 km/h on a dry asphalt road with  $\mu$  of approximately 0.9. Figs. 12 and 13 show the differential torque generated by the constrained HCC for differential braking (AWD) and hybrid torque vectoring (FWD) constraints, respectively. It is clear that, in both scenarios, the solution for the constrained optimization problem is feasible at every time step, and the torque values are distributed on all the wheels for the corresponding maneuver. Fig. 14 shows the driver's steering input and velocity profile for a maneuver on a surface with coefficient of friction  $\mu = 0.4$  with improved DCI. Figs. 15 and 16 show the differential torque values generated by the constrained HCC for differential braking (AWD) and hybrid torque vectoring (FWD) constraints, respectively. These figures show that this method of handling constraints works well in practice. Both yaw rate and sideslip angle are compared with and without control. The desired yaw-rate profile is also shown. Clearly, the effect of adding constraints on the control is efficient in tracking the desired yaw rate, keeping the sideslip angle small. The vehicle motion was smooth on the desired path, and the measured yaw rate at the CG closely follows the

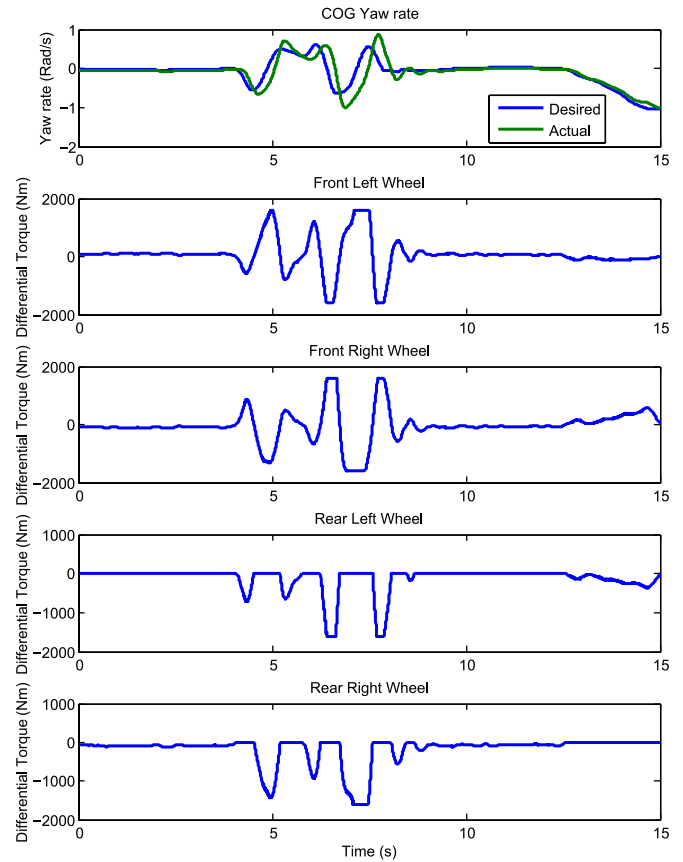


Fig. 13. Experimental result: Differential torque values generated by the hybrid torque vectoring (FWD) and differential braking on the rear wheels.

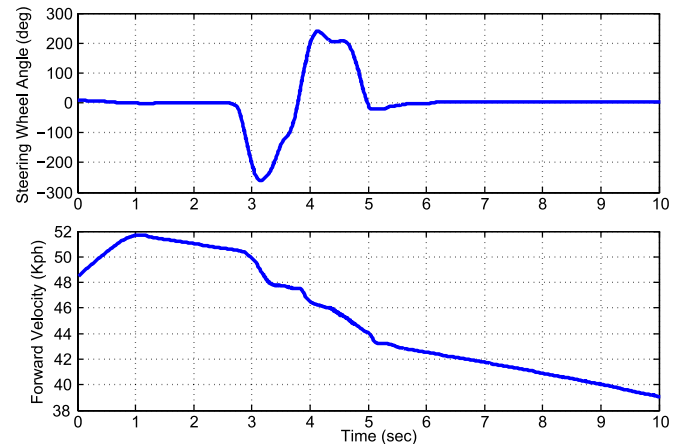


Fig. 14. Experimental input: Steering input and the velocity profile of the driver with the improved DCI.

desired yaw rate. All the results shown for real-time yaw rate is raw data directly measured by IMU sensor. Direct calculations were used in HCC, and no filters are used in the experiments. Fortunately, the sensors loaded on our vehicles are working properly, and the existing noise is not that significant.

## IX. CONCLUSION

In this paper, we have proposed an approach to handle linear constraints with HCC optimization. The HCC optimization is subjected to constraints on the applicable differential torque,

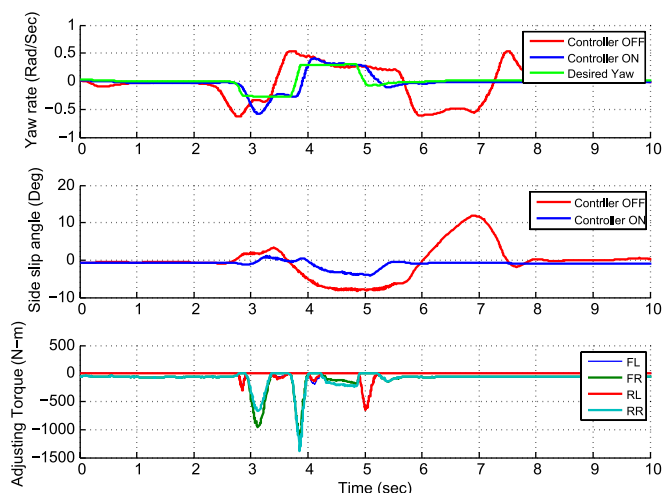


Fig. 15. Experimental result: Yaw rate (with and without control versus desired), sideslip angle (with and without control), and the adjusted torque values with improved DCI and differential braking.

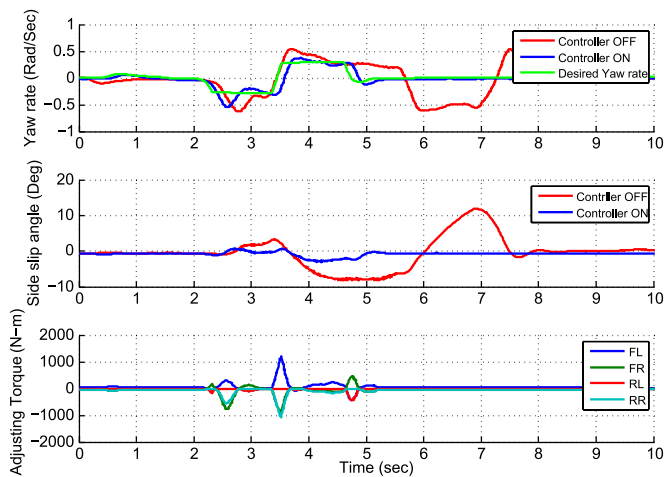


Fig. 16. Experimental result: Yaw rate (with and without control versus desired), sideslip angle (with and without control), and the adjusted torque with improved DCI and hybrid torque vectoring (FWD) in the front wheels and differential braking in the rear wheels.

and the resulting constrained optimization problem is solved numerically. This technique of adding constraints to the HCC optimization can be applied in a number of ways. Two applications of adding constraints to HCC are described and illustrated, with results from both simulations and experiments. The results indicate that fast numerical methods can be used in real-time applications. The proposed constrained HCC approach can be applied to conventional cars that do not have electric motors for actuation. The hypothesis behind this statement is that, instead of electric motors for actuation on the front wheels, differential braking could be applied on the rear wheels that has the same effect.

REFERENCES

[1] M. Nagai, Y. Hirano, and S. Yamanaka, "Integrated control of active rear wheel steering and direct yaw moment control," *Vehicle Syst. Dyn.*, vol. 27, no. 5, pp. 357–370, 1997.  
 [2] E. Ono, Y. Hattori, Y. Muragishi, and K. Koibuchi, "Vehicle dynamics integrated control for four-wheel-distributed steering and four-wheel-

distributed traction/braking systems," *Vehicle Syst. Dyn.*, vol. 44, no. 2, pp. 139–151, 2006.  
 [3] C. March and T. Shim, "Integrated control of suspension and front steering to enhance vehicle handling," *Proc. IMechE D, J. Automobile Eng.*, vol. 221, pp. 377–391, Apr. 2007.  
 [4] D. Li and F. Yu, "A novel integrated vehicle chassis controller coordinating direct Yaw moment control and active steering," Soc. Automotive Eng., Warrendale, PA, USA, Tech. Paper 2007-01-3642, 2007.  
 [5] E. Ono *et al.*, "Vehicle integrated control for steering and traction systems mu-synthesis," *Automatica*, vol. 30, no. 11, pp. 1639–1647, 1994.  
 [6] Y. Hattori, "Optimum vehicle dynamics control based on tire driving and braking forces," *Modeling, Anal. Control Methods Improving Vehicle, R&D Rev. Toyota CRDL*, vol. 38, no. 4, pp. 23–29, 2003.  
 [7] V. Pylypchuk, S.-K. Chen, N. Moshchuk, and B. Litkouhi, "Slip-based holistic corner control," in *Proc. ASME Int. World Congr. Expo.*, Denver, CO, USA, 2011, pp. 337–342.  
 [8] V. Pylypchuk, S.-K. Chen, Y. Ghoneim, N. Moshchuk, and B. Litkouhi, "Tire force based holistic corner control," in *Proc. ASME Int. World Congr. Expo.*, Houston, TX, USA, 2012, pp. 133–140.  
 [9] Y. A. Ghoneim, S.-K. Chen, V. Pylypchuk, N. K. Moshchuk, and B. Litkouhi, "Real-Time Allocation of Actuator Torque in a Vehicle," US Patent 8 655 528 B2, Jan. 31, 2011.  
 [10] S. Fallah, A. Khajepour, B. Fidan, S.-K. Chen, and B. Litkouhi, "Vehicle optimal torque vectoring using state-derivative feedback and linear matrix inequality," *IEEE Trans. Veh. Technol.*, vol. 62, no. 4, pp. 1540–1552, May 2013.  
 [11] D. Kasinathan, A. Khajepour, S.-K. Chen, and B. Litkouhi, "Constrained holistic cornering control," in *Proc. IEEE Amer. Control Conf.*, Portland, OR, USA, Jun. 4–6, 2014, pp. 3899–3904.  
 [12] S. Boyd and L. Vandenberghe, *Convex Optimization*. New York, NY, USA: Cambridge Univ. Press, 2004.  
 [13] J. Nocedal and S. J. Wright, *Numerical Optimization*. New York, NY, USA: Springer-Verlag, 1999.  
 [14] D. Luenberger, *Linear and Nonlinear Programming*. Reading, MA, USA: Addison-Wesley, 1984.  
 [15] I. Owadally, "An improved closed-form solution for the constrained minimization of the root of a quadratic functional," *J. Comput. Appl. Math.*, vol. 236, no. 17, pp. 4428–4435, Nov. 2012.  
 [16] H. J. Ferreau, P. Ortner, P. Langthaler, L. del Re, and M. Diehl, "Predictive control of a real-world Diesel engine using an extended online active set strategy," *Annu. Rev. Control*, vol. 31, no. 2, pp. 293–301, 2007.  
 [17] N. Gould and P. Toint, "Preprocessing for quadratic programming," *Math. Program., Ser. B*, vol. 100, no. 1, pp. 95–132, May 2004.  
 [18] P. E. Gill, W. Murray, and M. Wright, *Numerical Linear Algebra and Optimization*. Reading, MA, USA: Addison-Wesley, 1991.  
 [19] F. Delbos and J. Gilbert, "Global linear convergence of an augmented Lagrangian algorithm for solving convex quadratic optimization problems," *J. Convex Anal.*, vol. 12, no. 1, pp. 45–69, 2005.  
 [20] J. J. Mor and D. C. Sorensen, "Computing a trust region step," *SIAM J. Sci. Statist. Comput.*, vol. 4, no. 3, pp. 553–572, 1983.  
 [21] T. D. Gillespie, *Fundamentals of Vehicle Dynamics*. Warrendale, PA, USA: Soc. Automotive Eng., 1992.  
 [22] A. van Zanten, "Bosch ESP systems: 5 years of experience," Soc. Automotive Eng., Warrendale, PA, USA, Tech. Paper 2000-01-1633, 2000. [Online]. Available: doi: 10.4271/2000-01-1633  
 [23] K. Kitajima and H. Peng, "H $\infty$  control for integrated side-slip, roll and Yaw controls for ground vehicles," in *Proc. AVEC 5th Int. Symp. Adv. Vehicle Control*, 2000, pp. 1–8.  
 [24] W. Cho, J. Choi, C. Kim, S. Choi, and K. Yi, "Unified chassis control for the improvement of agility, maneuverability, and lateral stability," *IEEE Trans. Veh. Technol.*, vol. 61, no. 3, pp. 1008–1020, Mar. 2012.  
 [25] L. De Novellis, A. Sorniotti, and P. Gruber, "Optimal wheel torque distribution for a four-wheel-drive fully electric vehicle," *Soc. Automotive Eng. Int. J. Passenger Cars-Mech. Syst.*, vol. 6, no. 1, pp. 128–136, 2013.  
 [26] L. De Novellis, A. Sorniotti, P. Gruber, and A. Pennycott, "Comparison of feedback control techniques for torque-vectoring control of fully electric vehicles," *IEEE Trans. Veh. Technol.*, vol. 63, no. 8, pp. 3612–3623, Oct. 2014.  
 [27] A. Pennycott, L. De Novellis, A. Sorniotti, and P. Gruber, "The application of control and wheel torque allocation techniques to driving modes for fully electric vehicles," *SAE Int. J. Passenger Cars-Mech. Syst.*, vol. 7, no. 2, pp. 488–496, 2014.  
 [28] A. Pennycott, L. De Novellis, P. Gruber, and A. Sorniotti, "Optimal braking force allocation for a four wheel drive fully electric vehicle," *J. Syst. Control Eng.*, vol. 228, no. 8, pp. 621–628, 2014.

- [29] T. Goggia *et al.*, "Integral sliding mode for the torque-vectoring control of fully electric vehicles: Theoretical design and experimental assessment," *IEEE Trans. Veh. Technol.*, vol. 64, no. 5, pp. 1701–1715, May 2015.
- [30] O. Barbarisi, G. Palmieri, S. Scala, and L. Glielmo, "LTV-MPC for yaw rate control and side slip control with dynamically constrained differential braking," *Eur. J. Control*, vol. 15, no. 3/4, pp. 468–479, 2009.
- [31] M. Canale and L. Fagiano, "Vehicle yaw control using a fast NMPC approach," in *Proc. IEEE 47th CDC*, Dec. 2008, pp. 5360–5365.
- [32] S. Di Cairano, H. E. Tseng, D. Bernardini, and A. Bemporad, "Vehicle Yaw stability control by coordinated active front steering and differential braking in the tire sideslip angles domain," *IEEE Trans. Control Syst. Technol.*, vol. 21, no. 4, pp. 1236–1248, Jul. 2013.
- [33] J. Kang, Y. Kyongsu, and H. Heo, "Control allocation based optimal torque vectoring for 4WD electric vehicle," Soc. Automotive Eng., Warrendale, PA, USA, Tech. Paper 2012-01-0246, 2012.
- [34] D. H. Kim, J. M. Kim, S. H. Hwang, and H. S. Kim, "Optimal brake torque distribution for a four-wheeldrive hybrid electric vehicle stability enhancement," *Proc. Inst. Mech. Eng. D, J. Automobile Eng.*, vol. 221, no. 11, pp. 1357–1366, 2007.
- [35] H. Kopka and P. W. Daly, *A Guide to LaTeX*, 3rd ed. Harlow, U.K.: Addison-Wesley, 1999.



**Dhanaraja Kasinathan** received the B.E. degree in electrical engineering and the M.Sc. degree in mathematics from Birla Institute of Technology and Science, Pilani, India, and the Ph.D. degree in applied mathematics from the University of Waterloo, Waterloo, ON, Canada.

From 2005 to 2007, he was an Associate Engineer with Broadcom Research India Pvt. Ltd. He was also a Postdoctoral Fellow with the Department of Mechanical and Mechatronics Engineering, University of Waterloo. He is currently with the United

Technologies Research Center, Cork, Ireland, as a Senior Research Scientist, working on optimization and control of high-performance buildings. His research interests include control theory, optimization and control, numerical methods for partial differential equations, parallel computing, vehicle control, stability analysis of nonlinear dynamical systems, and control applications in building systems.



**Alireza Kasaiezadeh** received the B.Sc. and M.Sc. degrees from Sharif University of Technology, Tehran, Iran, and the Ph.D. degree in mechanical and mechatronic engineering from the University of Waterloo, Waterloo, ON, Canada.

He did a two-year postdoctoral fellowship and was a Research Assistant Professor with the University of Waterloo. He is currently a Senior Researcher with GM Technical Center, General Motors Company, Warren, MI, USA, where he is working in the area of automated driving and vehicle

control. He has more than 14 years of industrial experience in the automotive industry and, in particular, in active safety systems, chassis control system design, and field testing. His research interests include automated driving, vehicle dynamics, control and optimization.



**Andy Wong** received the Bachelor's degree and the Master's degree in mechanical engineering, specializing in mechatronics, from the University of Waterloo, Waterloo, ON, Canada.

He is currently with the Department of Mechanical and Mechatronics Engineering, University of Waterloo. His research interests include vehicle dynamics, autonomous path planning, and robotics.



**Amir Khajepour** received the B.Sc. and M.Sc. degrees from Ferdowsi and Sharif University, Iran, in 1989 and 1991 and the Ph.D. degree from the University of Waterloo, ON, Canada, in 1996.

He is a Professor and Canada Research Chair of "Mechatronic Vehicle Systems" with the Department of Mechanical and Mechatronics Engineering, University of Waterloo. He is an expert in systems modeling and control of dynamic systems and has developed an extensive research program in several key multidisciplinary areas. His research has resulted

in several patents and technology transfers, over 320 journal and conference publications, and five books and seven book chapters.

Dr. Khajepour received the Engineering Medal from Professional Engineering Ontario, three best paper awards, and is a fellow of the Engineering Institute of Canada and the American and Canadian Society of Mechanical Engineering.



**Shih-Ken Chen** received the B.S. degree from National Taiwan University, Taipei, Taiwan, in 1985; the M.S. degree in mechanical engineering from the University of Wisconsin–Madison, Madison, WI, USA, in 1990; and the Ph.D. degree in mechanical engineering from Massachusetts Institute of Technology, Cambridge, MA, USA, in 1996.

He then joined the Research and Development Center, General Motors Corporation. He is currently a Staff Researcher with the GM Technical Center, General Motors Company, Warren, MI, USA. His

previous work includes collision avoidance systems, electronic stability control, active all-wheel-steer control, and rollover avoidance. His current research interests include holistic chassis and vehicle control for both conventional driveline and electric driveline, driver-in-the-loop vehicle control, and vehicle active safety system and automated driving.



**Bakhtiar Litkouhi** received the B.Sc. degree in mechanical engineering from Arya-Mehr (Sharif) University of Technology, Iran and the M.Sc. degree in applied mathematics and the Ph.D. degree in systems science, specializing in control, both from Michigan State University, East Lansing, MI, USA.

He was an Assistant Professor with Oakland University, Rochester, MI, USA. He has served as the Program Manager for several large-scale projects in automated and intelligent vehicle systems, human-machine interface, and integrated vehicle control,

where he has made many contributions through numerous patents, publications, and presentations. He is currently the Manager of Automated Driving and Vehicle Control Systems, General Motors Global Research and Development, Warren, MI, USA. In addition to his current responsibilities, he is a board member of the Intelligent Transportation Society of Michigan, a member of the Board of Directors of the Waterloo Center for Automotive Research (WatCAR), and the Program Manager of GM–Carnegie Mellon University Autonomous Driving Collaborative Research Lab.